DNS of Rising Bubbles Using VOF and Balanced Force Surface Tension

Hendrik Weking, Jan Schlottke, Markus Boger, Philipp Rauschenberger, Bernhard Weigand, Claus-Dieter Munz

Abstract The rise behavior of small bubbles in a quiescent environment has been investigated by direct numerical simulation (DNS) using the Volume of Fluid (VOF) method and surface tension modeling based on the balanced force approach. The origin of spurious currents using standard (CSF, CSS) models is shown in detail, emphasis is put on the spatial discretization and the calculation of local curvatures. The effect of the new surface tension model on the resulting rise behavior for different bubble diameters is presented.

1 Introduction

Bubbly flows play an important role in many industrial applications such as fermentation reactors floating or loop reactors. The improvement of the efficiency of these reactors requires a deeper understanding of the rise behavior of gaseous bubbles. Therefore this issue has been the topic of many experimental and numerical studies, e.g. [12, 18, 9]. A wide range of contributions to the subject of the motion of bubbles, drops and particles is contained in the book of Clift, Grace and Weber [2]. Koebe [10] employed the ITLR inhouse code FS3D to investigate the rise of bubbles. The FS3D code is also used in this investigation to simulate rising air bubbles in quiescent water. The treatment of fluid interfaces is a crucial factor for the direct numerical simulation (DNS) of two-phase flow. As the interface represents a

Hendrik Weking, Jan Schlottke, Philipp Rauschenberger, Bernhard Weigand
Institut für Thermodynamik der Luft- und Raumfahrt (ITLR), Universität Stuttgart, Pfaffenwaldring 31, 70569 Stuttgart, Germany
e-mail: hendrik.weking@itlr.uni-stuttgart.de

Markus Boger, Claus-Dieter Munz
Institut für Aerodynamik und Gasdynamik (IAG), Universität Stuttgart, Pfaffenwaldring 21, 70569 Stuttgart, Germany
e-mail: boger@iag.uni-stuttgart.de

M. Resch et al. (eds.), *High Performance Computing on Vector Systems 2010*,
DOI 10.1007/978-3-642-11851-7_13,

discontinuity separating the two fluids, jump conditions have to be applied. Using the so called one-fluid formulation, one is able to work with a single set of equations for the whole flow domain. The coupling of the fluids at the interface is taken into account by the use of variable material properties. Moreover, the Navier-Stokes equations contain an additional volume force term for the surface tension, which is directly linked to the interface location via a delta function concentrated on the surface. From a physical point of view the surface force is balanced by the pressure jump across the interface. As the volume force is only different from zero at the interface, no additional jump conditions with regard to momentum conservation have to be applied.

In general, surface tension is numerically approximated by a volume force using a continuum model. Applying the widespread continuum surface force (CSF, [1]) or continuum surface stress (CSS, [11]) model, many DNS codes suffer from unphysical parasitic currents in the vicinity of the surface.

In particular, the occurrence of spurious currents prevents the investigation of small bubbles with diameters $d_e < 2$ mm. For these cases the numerically induced, parasitic accelerations increase the magnitude of the physical, gravity driven accelerations and thus no benefit can be extracted from such simulations.

In order to overcome this issue, many efforts have been taken by various researchers. For two dimensional computations Meier et al. [13] proposed a method to determine curvature more accurately using an estimator function, tuned with a least-squares-fit against precomputed reference data. An approximation of the surface tension based on spline interpolants was presented by Ginzburg and Wittum [5]. For 3D calculations, Renardy and Renardy [16] developed the PROST algorithm (parabolic reconstruction of surface tension) and Jafari et al. [8] presented the PCIL method (pressure calculation based on the interface location) where the pressure forces at the interfacial cell faces are calculated according to the pressure imposed by each fluid on the portion of the cell face that is occupied by that fluid. This list is far from being complete as there are many other approaches aiming at the reduction of parasitic currents.

The method used for the calculations presented in this paper is based on the balanced force approach by François et al. [4]. Starting from the original CSF model of Brackbill et al. [1] only minor changes are needed, mainly linked to curvature calculation which we choose to be evaluated according to Popinet [15].

The outline of the paper is as follows. We firstly introduce the governing equations for the DNS of two-phase flows, as they are used in the framework of the FS3D code. The following section is dedicated to the calculation of surface tension. In this context the origin of parasitic currents is discussed. This includes on the one hand the correct discretization of the surface tension terms in order to have a so called balanced-force algorithm. On the other hand, the issue of curvature estimation has also to be taken into account and for that we are using a height function method. The results section comprises various calculations on the rise behavior of small bubbles, comparing the results of the two standard models (CSF, CSS) and the new surface tension model (CSF-BHF).

2 Governing Equations

2.1 Continuity and Navier-Stokes Equations

The incompressible two phase flow is described by the continuity equation and the Navier-Stokes equations. Using the one-fluid formulation, the continuity equation and the momentum equations have the following form

$$\nabla \cdot \mathbf{u} = 0, \tag{1}$$

$$\frac{\partial(\rho \mathbf{u})}{\partial t} + \nabla \cdot (\rho \mathbf{u}) \otimes \mathbf{u} = -\nabla p + \rho \mathbf{k} + \nabla \cdot \mu[(\nabla \mathbf{u} + (\nabla \mathbf{u})^T)] + \mathbf{f}_\gamma \delta_S. \tag{2}$$

Here $\mathbf{u}$ represents the velocity, ρ denotes the density, p is the pressure, t is the time, μ is the dynamic viscosity, $\rho \mathbf{k}$ takes into account body forces, the term $\mathbf{f}_\gamma$ is a body force that represents the influence of surface tension in the vicinity of the interface and δ_S is a delta function concentrated on the surface.

These equations resemble the conservation equations for one phase flows with the exception of the appearance of the volume force $\mathbf{f}_\gamma$ on the right-hand side of the momentum equations in Eq. 2. This approach is called the one-fluid formulation and it allows the use of a single set of equations in the whole flow domain. In the absence of mass transfer, there is no need of establishing any additional jump conditions at the fluid interface as they are implicitly taken into account by this formulation. The coupling of the two fluids is provided by variable material properties ρ and μ. They are chosen according to the fluid occupying a grid cell. At the interface the volume force $\mathbf{f}_\gamma$ comes into play for taking into account the effects of surface tension.

2.2 Interface Tracking by the VOF Method

The interface tracking is based on the volume of fluid (VOF) method developed by Hirt et al. [7]. For the representation of the phases, an additional variable f is introduced

$$f = \begin{cases} 0 & \text{in the gaseous phase,} \\ 0 < f < 1 & \text{in cells containing a part of the interface,} \\ 1 & \text{in the liquid phase,} \end{cases} \tag{3}$$

which represents the volume fraction of the liquid phase. A two dimensional example is given in Fig. 1. According to the one-fluid formulation, the above mentioned change in material properties is based on the volume fraction variable f

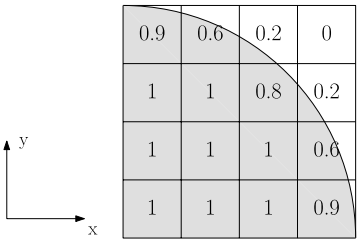

Fig. 1 Fluid representation by the volume fraction f variable

$$\rho(\mathbf{x},t) = \rho_g + (\rho_l - \rho_g) \cdot f(\mathbf{x},t), \tag{4}$$

$$\mu(\mathbf{x},t) = \mu_g + (\mu_l - \mu_g) \cdot f(\mathbf{x},t), \tag{5}$$

where the indices l and g denote the liquid and the gaseous phase, respectively.

The movement of the interface is tracked via the transport of the volume fraction f by

$$\frac{\partial f}{\partial t} + \nabla \cdot (f\mathbf{u}) = 0. \tag{6}$$

While advecting the volume fraction f, one is interested in keeping the interface sharply resolved. Therefore at every time step the interface is reconstructed based on a PLIC (piecewise linear interface calculation) algorithm (see e.g. [17]). This geometrical reconstruction is used to determine the liquid and gaseous fluxes across the cell faces and it prevents the interface from being smeared across several grid cells during the advection.

2.3 Moving Frame of Reference

A moving frame of reference is employed to investigate the bubble motion over a larger time scale and thus over a longer rising path without a large computational domain and the resulting computational effort as presented in [19]. This technique induces a counterflow in the domain which is adapted dynamically over time. Therefore the motion of the center of mass of the bubble is considered as a damped oscillation of a point mass around its initial position. Depending on the displacement and the velocity of the center of mass of the gaseous phase a correction body force $\rho\mathbf{k}_c$ is imposed to the flow field by adding it to the right-hand side of Eq. 2, inducing the counter flow in the computational domain. This keeps the bubble close to its initial position, or from the view of a resting observer, moves the whole domain along with the bubble. This correction force is computed for all three spatial directions in every timestep by

$$\mathbf{k}_c = 2\omega \frac{\mathbf{P}_g}{m^*} + c_2 \omega^2 \Delta \mathbf{x}_g, \tag{7}$$

with the momentum of the bubble $\mathbf{P}_g$ divided by the bubble virtual mass $m^* = m_g\left(\rho_f/\rho_g\right)$ and the displacement vector $\Delta\mathbf{x}_g$. The momentum and the displacement vector refer to the moving frame of reference. To avoid a build up in the displacement the value of c_2 is switched from 1 to 0 if the center of mass is approaching the initial position. The angular frequency governing the hardness of the damping and thus the magnitude of the oscillation around the initial position is chosen to be

$$\omega = c_1\sqrt{\frac{\rho_f}{\rho_g}}\pi\omega_{res} = c_1\sqrt{\frac{\rho_f}{\rho_g}}\pi\sqrt{\frac{12\sigma}{d_e^3\rho_f}}, \tag{8}$$

where ω_{res} is the first resonance mode of the bubble surface. ω_{res} is multiplied by π to avoid that ω becomes a higher mode of that surface resonance frequency and thus prevent a build up of surface oscillations which could destroy the free surface. A value of $c_1 = 10$ was chosen in this study. Note, that this formulation does not fix the bubble at the start position but allows a displacement.

3 Surface Tension

At an interface separating two immiscible fluids a pressure jump

$$p_2 - p_1 \equiv \Delta p = \sigma\kappa, \tag{9}$$

appears according to the Young-Laplace equation. Here σ is the surface tension coefficient and κ represents the curvature. Hence, surface tension is directly proportional to the curvature κ. This jump in pressure has to be considered when simulating two-phase flows. Therefore, different models have been developed in order to include surface tension at the interface. As it is obvious from Eq. 2, surface tension is accounted for as a volume force in the momentum equations. The corresponding force $\mathbf{f}_\gamma$ on the right-hand side of the equation is only present at the interface while it vanishes in grid cells away from the interface.

3.1 The Continuum Surface Force (CSF) Model

The basic idea of the continuum surface force (CSF) model introduced by Brackbill et al. [1] can be described as follows. Instead of considering the fluid interface as a sharp discontinuity, one supposes a smooth transition from one fluid to another. The interface is considered to have a finite thickness of $O(h)$, corresponding to the smallest length scale h resolvable by the computational mesh. Consequently, surface tension is also considered to be of continuous nature and it acts everywhere within the transition region. Brackbill and coworkers propose to calculate $\mathbf{f}_\gamma$ by

$$\mathbf{f}_\gamma = \sigma \kappa \nabla f. \tag{10}$$

This corresponds to a dispersion of the surface tension across the transition region, using the gradient of the volume fraction variable f to weight the dispersed volume force. Implementing this approach in a CFD code, one has to consider the

1. spatial discretization of Eq. 10,
2. estimation of curvature κ,

in order to prevent parasitic currents. The following sections will provide a discussion on both aspects.

3.2 Balanced-Force Algorithm

Looking at the spatial discretization, the variables are stored on a staggered grid arrangement according to [6]. On such a MAC (marker-and-cell) grid, the scalar variables (f, p) are stored at the cell centers, while the velocities are stored at the centers of the cell faces. In order to guarantee an accurate, balanced-force discretization, according to [4], the surface tension terms (cf. Eq. 10) have to be calculated at the center of the cell faces. Furthermore, it is of crucial importance that pressure and surface tension are discretized in the same way.

Moreover, special care has to be taken in order to evaluate the gradient ∇f. For the original CSF method, according to [1], the evaluation of the gradient is performed on a stencil of 18 cells for 3D calculations. For explanation purposes Fig. 2 illustrates a two dimensional example. Here, the gradients at the cell face centers of row (j) are given by the corresponding values in red. Taking the face at $(i+1/2)$ as an example, the gradient $\nabla f_{x_{i+1/2,j}}$ is based on the gradients in the rows $(j-1), (j), (j+1)$ that are calculated on the basis of the cells adjacent to the face $(i+1/2)$ respectively, e.g. $\tilde{\nabla} f_{x_{i+1/2,j}} = \frac{f_{(i+1,j)} - f_{(i,j)}}{\Delta x}$ for row (j). Here, $\tilde{\nabla}$ designates the local gradient with respect to the cell face. Afterwards, the gradient at the position $x_{i+1/2,j}$ is obtained as

$$\nabla f_{x_{i+1/2,j}} = \frac{1}{4}\left(\tilde{\nabla} f_{x_{i+1/2,j-1}} + 2\tilde{\nabla} f_{x_{i+1/2,j}} + \tilde{\nabla} f_{x_{i+1/2,j+1}}\right). \tag{11}$$

This leads to a total stencil for cell (i, j) that is surrounded by the dashed lines in Fig. 2. It is obvious that the above discretization implies a coupling of the rows $(j-1), (j), (j+1)$ for the surface tension calculation via the evaluation of the gradients. Having a closer look at the discretization of the Poisson equation used for the calculation of p, in x direction for the cell (i, j), one finds

$$\frac{1}{\Delta x}\left(\frac{p_{(i+1,j)} - p_{(i,j)}}{\rho_{(i+1/2,j)}} - \frac{p_{(i,j)} - p_{(i-1,j)}}{\rho_{(i-1/2,j)}}\right) = \frac{\tilde{\mathbf{u}}_{(i+1/2,j)} - \tilde{\mathbf{u}}_{(i-1/2,j)}}{\Delta t}. \tag{12}$$

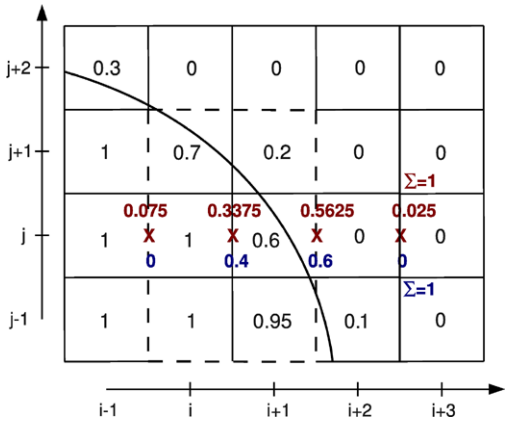

Fig. 2 Evaluation of ∇f based on a stencil of 6 cells (red) and on the direct neighbors of the cell face (blue). The box surrounded by the dashed lines marks the 6 cell stencil for the cell face $(i+1/2, j)$

Here it is clearly visible that all pressure values are taken from row (j). As for the above mentioned discretization of the surface tension used to evaluate the velocity $\tilde{\mathbf{u}}$, the rows $(j-1), (j+1)$ are also included via the gradient evaluation. We found this coupling to be one of the causes for the parasitic currents using the CSF implementation in FS3D. Therefore we changed the gradient evaluation to a more local formulation only taking into account direct neighbors of the cell faces. This leads for the cell face $(i+1/2, j)$ to

$$\nabla f_{x_{i+1/2,j}} = \tilde{\nabla} f_{x_{i+1/2,j}} = \frac{f_{(i+1,j)} - f_{(i,j)}}{\Delta x}. \tag{13}$$

Returning to Fig. 2, the two approaches can be compared directly. According to the two methods, the gradients are given for the previous method (red) and the local approach (blue) in row (j). While the transition from one fluid to the other is spread over four cell faces with the previous approach, the local approach only uses two cell faces to disperse the jump in pressure.

In 3D, the gradients for the different spatial directions are evaluated in an analogous way, only taking into account direct neighbors of the respective cell face.

Besides the discretization of the surface tension force (Eq. 10), the correct estimation of surface curvature is very important and shall be discussed in the following section.

3.3 Curvature Estimation

In the context of the VOF method, difficulties in determining topology information like normal vectors and curvature are due to the discrete nature of the volume

fractions. Contrary to a level-set function, the VOF field is not smooth and thus the correct curvature as the second derivative is hard to obtain. Direct calculation of curvature from the given volume fractions leads to high frequency (order of the grid) errors (aliasing error, [3]). This is why most CSF implementations do a smoothing of the VOF field prior to the calculation of curvature. In addition, this error does not vanish with grid refinement.

For the method presented here, the curvature is calculated based on a height function approach, coupled to a local paraboloid fitting if the grid resolution is not sufficient. The procedure is inspired by the article of Popinet [15]. The height function approach is a geometrical one. The stencil used to determine the local height is not fixed (as used by e.g. [4]), but adapts itself to capture the local topology in an optimal way.

As already mentioned, grid resolution does not always permit the determination of curvature via the height function approach. This is the case for highly curved topology, e.g. during breakup, or in case of very coarse grids. Local curvature is then determined by fitting a paraboloid to known points on the surface. These points can either originate from local heights or the barycenters of the reconstructed surface (using PLIC) are used for this purpose. Once the paraboloid, given by

$$f(a_i, \mathbf{x}) = a_0 x^2 + a_1 y^2 + a_2 xy + a_3 x + a_4 y + a_5, \tag{14}$$

is fitted (via least squares fit) to these points, the curvature can easily be calculated as the second derivative,

$$\kappa = 2\frac{a_0(1+a_4^2) + a_1(1+a_3^2) - a_2 a_3 a_4}{(1+a_3^2+a_4^2)^{3/2}}. \tag{15}$$

4 Numerical Setup

Employing the moving frame of reference it is not necessary to discretize the entire rising path. The computational domain can be reduced to a small frame around the bubble, as shown in Fig. 3. On the upper side of the 3D computational domain a uniform inflow condition is employed. On all other boundaries, including the outflow, a continuous (Neumann) condition is used. To oppress undesired back flow a damping zone is placed in front of the outflow boundary. The gravity pointing towards the outflow boundary leads to a strong acceleration of the liquid, which 'falls' out of the domain, taking the bubble with it. This can be avoided by replacing gravity by buoyancy in the momentum equation. In the presented study a variety of bubble diameters were investigated. Therefore the extent of the computational domain varies depending on the initial bubble diameter. The computational domain has an overall length of 20 bubble diameters in the direction of the main flow and 10 bubble diameters between the lateral boundaries. The resolution is chosen to be 512 cells in main flow direction and 256 cells in the lateral direction, which makes about $33 \cdot 10^6$

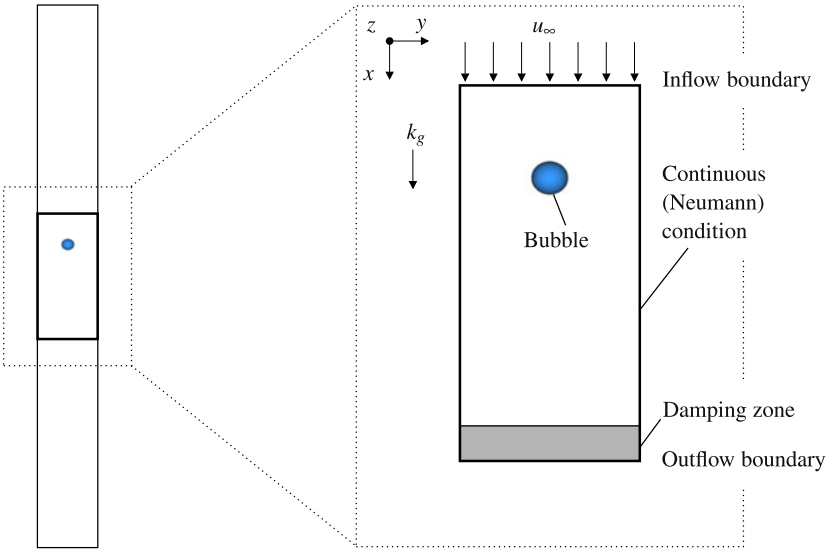

Fig. 3 Numerical setup and coordinate system

computational cells in the whole domain. At this resolution the equivalent bubble diameter is resolved by 25.6 cells.

In all cases the air bubble is initialized as a stationary sphere surrounded by quiescent water at a distance of 5 bubble diameters away from the inflow and the lateral boundaries.

5 Results: Rise Behavior of Bubbles

5.1 Reduction of Spurious Currents

The simulation of small bubbles with an equivalent diameter $d_e < 2$ mm leads to unphysical results using CSF and CSS models. In these cases the spurious currents induced by the high curvature of the interface are no longer negligible. Figure 4 shows the velocity field in a cut plane through the bubble center for $d_e = 1$ mm (left) and $d_e = 2$ mm (right) computed by the CSF, CSS and the new CSF-BHF model. For both bubble diameters the results using the CSF model are strongly influenced by spurious currents. The velocity field computed using the CSS model is apparently free from disturbances caused by spurious currents in case of the 2 mm bubble whereas for the 1 mm case such disturbances appear at the top and the bottom of the bubble. In contrast, the velocity field obtained using the new model is free from spurious currents for both bubble diameters.

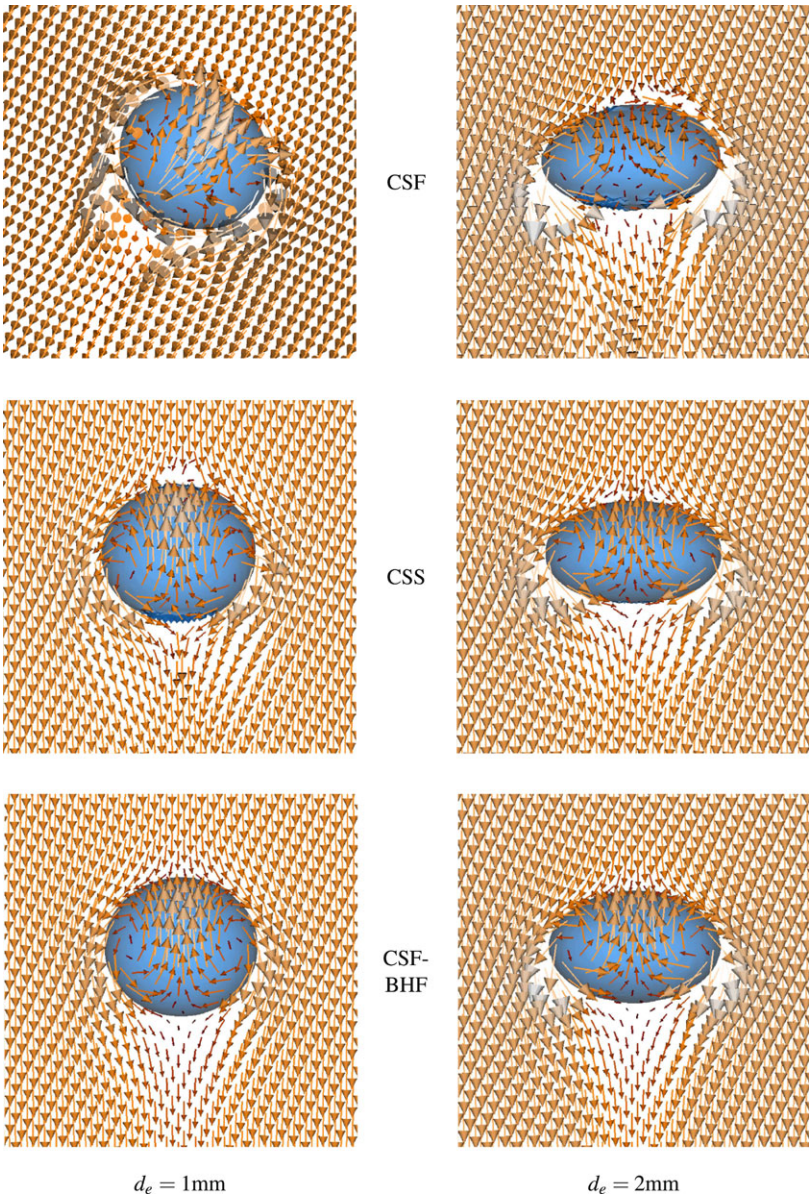

Fig. 4 Velocity field using CSF, CSS and CSF-BHF model for $d_e = 1$ mm (left) and $d_e = 2$ mm (right)

The corresponding development of the rise velocity is plotted in Fig. 5. For the 1 mm case (left) both, the CSF and CSS model, fail to predict a smooth trend due to spurious currents in contrast to the CSF-BHF model. Although the mean rise velocity computed using the CSS model is in the same magnitude as the velocity

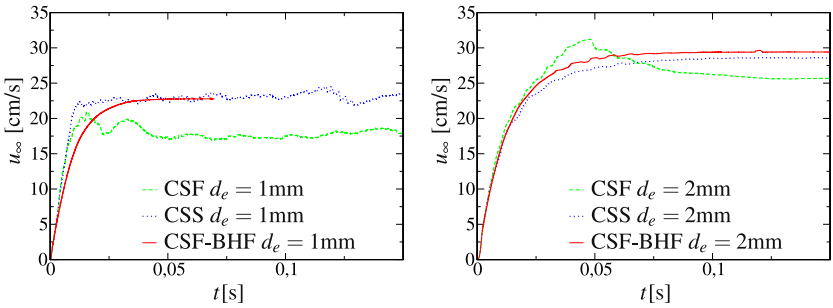

Fig. 5 Comparison of rise velocity using CSF, CSS and CSF-BHF model for $d_e = 1$ mm (left) and $d_e = 2$ mm (right)

gained by the CSF-BHF model, strong oscillations occur due to the nondirectional disturbances of the spurious currents. To demonstrate the influence of the spurious currents near the free surface the ration of the instantaneous interface area to the initial area of the spherical bubble A/A_0, which is the degree of deformation of the bubble, is shown in Fig. 6 (left).

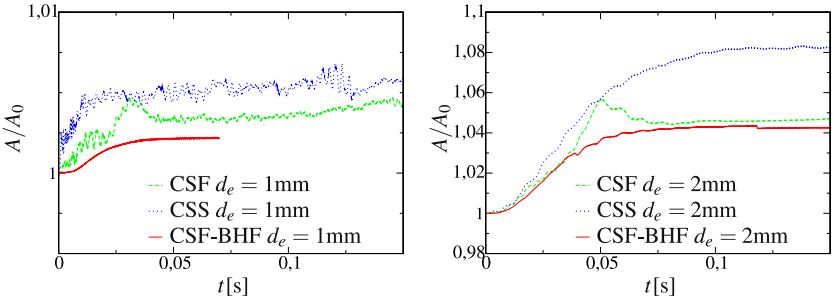

Fig. 6 Comparison of interface area using CSF, CSS and new CSF-BHF model for $d_e = 1$ mm (left) and $d_e = 2$ mm (right)

Only the new model is capable to reproduce a smooth deformation from the sphere to an elliptic shape as the bubble rises. In case of a 2 mm bubble (Fig. 5 right) the CSS and the new CSF-BHF model produce comparable results for the instantaneous rise velocity whereas the rise velocity computed using the CSF model first exceeds the velocity predicted by the other models and decreases to a lower level after this peak. The same peak is found regarding the instantaneous deformation in Fig. 6 (right).

5.2 Terminal Rise Velocity

At the start of the simulation the bubbles are initialized at zero velocity. After a short phase of acceleration, they reach a maximum rise velocity. In this phase the rising trajectory of the bubble stays rectilinear. Depending on its equivalent diameter the motion of the bubble can then turn into a zigzagging or spiraling path. In these cases, the terminal rise velocity is not the maximum velocity of the rectilinear part but the mean value of the 3D motion part. In the cases investigating 3D motion only occurred for $d_e > 3$ mm.

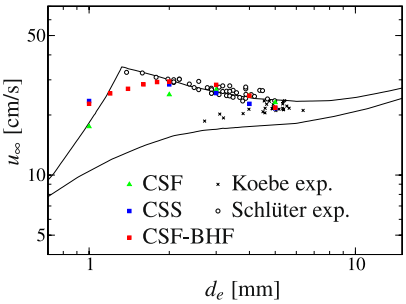

Fig. 7 Comparison of terminal rise velocity with experimental data

The results of the terminal rise velocity are plotted over the equivalent diameter in Fig. 7. The lines in the plot are taken from Clift et al. [2] and represent the terminal rise velocity for air bubbles in pure water (upper line) and in conterminated water (lower line). Regarding the terminal rise velocity the results of all surface tension models fit well with the experimental data measured by Koebe [9] and Schlüter [18] for $d_e \geq 3$ mm. In the region below 2 mm the new surface tension model underestimates the terminal rise velocity, the results are still between the two lines by Clift et al. [2]. The only exception is the 1 mm case where the velocity calculated is too high. Note, that the 1 mm case of the CSS model and the 1 mm and 2 mm cases of the CSF model are affected by spurious currents and are only plotted for the sake of completeness.

5.3 Bubble Shape

The deformation of a bubble is measured by the ratio of the bubble height to its width H/W after reaching the terminal velocity. Obviously, this can only be done when the bubbles develop to a rotational symmetric oblate shape, which is the case for a rectilinear trajectory. In the cases where a 3D rising path occurs, the bubbles develop an arbitrary time dependent shape. The deformation of the bubbles computed using the new model with an equivalent diameter $d_e \leq 2$ mm is presented in Fig. 8 as a

function of the Weber number

$$We = \frac{\rho_l d_e u_\infty^2}{\sigma}. \tag{16}$$

The Weber number is the ratio of the kinetic energy to the causing distortion to the surface energy available to resist it. The computed terminal rise velocity shown in Fig. 7 is chosen as the reference velocity u_∞. Figure 8 shows that for small equivalent diameters the simulated deformations match the correlation of Moore [14] for small distortions

$$H/W = \frac{1}{1 + \frac{9}{64} We + O(We^2)}. \tag{17}$$

For larger deformations and thus larger Weber numbers the numerical results deviate from that correlation.

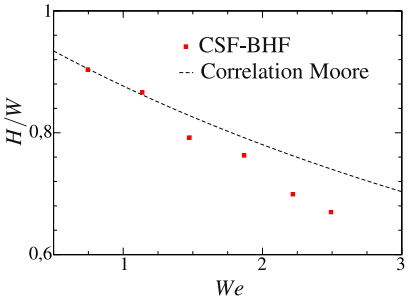

Fig. 8 Bubble deformation H/W for over Weber number computed with CSF-BHF

6 Conclusion

DNS of the rise behavior of small bubbles in a quiescent liquid using the volume of fluid (VOF) method has been presented. The use of an advanced surface tension model based on the balanced force approach and on the calculation of local curvature via height functions enables the investigation of bubbles with diameters smaller than 3 mm where unphysical spurious currents normally dominate the solution when using standard models (CSF, CSS). The predicted rise velocities and bubble deformation fit the experimental data and the correlations from literature. This approach demonstrates that DNS calculations can be used as 'numerical experiments' in order to understand detailed complicated two phase flow situations.

Acknowledgements The authors would like to thank the German Research Foundation (DFG) for financial support of the project within the Cluster of Excellence in Simulation Technology (EXC 310/1) at the University of Stuttgart and the PAK 119. Additionally the authors greatly appreciate

the *High Performance Computing Center Stuttgart* (HLRS) for support and computational time on the NEC-SX8 platform under the Grant No. FS3D/11142.

References

1. Brackbill, J.U., Kothe, D.B., Zemnach, C.: A continuum method for modeling surface tension. J. Comput. Phys. **100**, 335–354 (1992)
2. Clift, R., Grace, J.R., Weber, M.E.: Bubbles, Drops, and Particles. Dover Publications Inc., Mineola, New York, USA (2005)
3. Cummins, S.J., Francois,M.M., Kothe, D.B.: Estimating curvature from volume fractions. Comput. Struct. **83**, 425–434 (2005)
4. Francois, M.M., Cummins, S.J., Dendy, E.D., Kothe, D.B., Sicilian, J.M., Williams, M.W.: A balanced-force algorithm for continuous and sharp interfacial surface tension models within a volume tracking framework. J. Comput. Phys. **213**, 141–173 (2006)
5. Ginzburg, I., Wittum, G.: Two-Phase Flows on Interface Refined Grids Modeled with VOF, Staggered Finite Volumes, and Spline Interpolants. J. Comput. Phys. **166**, 302–335 (2001)
6. Harlow, F.H., Welch, J.E.: Numerical Calculation of Time-Dependent Viscous Incompressible Flow of Fluid with Free Surface. Phys. Fluids **8**, 2182–2189 (1965)
7. Hirt, C.W., Nichols, B.D.: Volume of fluid (VOF) method for the dynamics of free boundaries. J. Comput. Phys. **39**, 201–225 (1981)
8. Jafari, A., Shirani, E., Ashgriz, N.: An improved three-dimensional model for interface pressure calculations in free-surface flows. Int. J. Comput. Fluid Dyn. **21**, 87–97 (2007)
9. Koebe, M.: Numerische Simulation aufsteigender Blasen mit und ohne Stoffaustausch mittels der Volume of Fluid (VOF) Methode. PhD thesis, Lehrstuhl für Technische Chemie und Chemische Verfahrenstechnik, Universität Paderborn, Germany, (2004)
10. Koebe, M., Bothe, D., Prüss, J., Warnecke, H.J.: 3D Direct Numerical Simulation of Air Bubbles in Water at high Reynolds numbers. Proceedings of ASME FEDSM'02 (2002)
11. Lafaurie, B., Nardone, C., Scardovelli, R., Zaleski, S., Zanetti, G.: Modelling Merging and Fragmentation in Multiphase Flows with SURFER. J. Comput. Phys. **113**, 134–147 (1994)
12. Maxworthy, T., Gnann, C., Kürten, M., Durst, F.: Experiments on the rising of air bubbles in clean viscous liquids. J. Fluid Mech. **321**, 421–411 (1996)
13. Meier, M., Yadigaroglu, G., Smith, B.L.: A novel technique for including surface tension in PLIC-VOF methods. Eur. J. Mech. B. Fluids **21**, 61–73 (2002)
14. Moore, D.W.: The velocity of rise of distorted gas bubbles in a liquid of small viscosity. J. Fluid Mech. **23**, 749–766 (1965)
15. Popinet, S.: An accurate adaptive solver for surface-tension-driven interfacial flows. J. Comput. Phys. **228**, 5838–5866 (2009)
16. Renardy, Y., Renardy, M.: PROST: A Parabolic Reconstruction of Surface Tension for the Volume-of-Fluid Method. J. Comput. Phys. **183**, 400–421 (2002)
17. Rider, W.J., Kothe, D.B.: Reconstructing Volume Tracking. J. Comput. Phys. **141**, 112–152 (1998)
18. Schlüter, M.: Blasenbewegung in praxisrelevanten Zweiphasenströmungen. PhD thesis, Institut für Umweltverfahrenstechnik, Universität Bremen, Germany, (2002)
19. Weking, H., Huber, C., Weigand, B.: Direct Numerical Simulation of Single Gaseous Bubbles in Viscous Liquids. High Performance Computing in Science and Engineering '09. Springer, Berlin Heidelberg New York (2009)